CARBON 48 (2010) 3840–3845

available at www.sciencedirect.com

ScienceDirect

journal homepage: www.elsevier.com/locate/carbon

Catalyst rotation, twisting, and bending during multiwall carbon nanotube growth

Michael J. Behr, K. Andre Mkhoyan, Eray S. Aydil *

Department of Chemical Engineering & Materials Science, University of Minnesota, 151 Amundson Hall, 421 Washington Avenue SE, Minneapolis, MN 55455, USA

ARTICLE INFO

Article history:
Received 23 April 2010
Accepted 18 June 2010
Available online 25 June 2010

ABSTRACT

Internal crystalline structure of cementite catalyst particles located inside the base of multiwall carbon nanotubes was studied using nanoprobe convergent-beam electron diffraction. The catalyst particles are single crystalline but exhibit combinations of small-angle (~1°–3°) rotations, twists, and bends along their axial length between adjacent locations. Distortions are most severe away from the base up into the nanotube where the number of walls is large. Near the attachment point to the substrate, however, where few, if any graphene walls exist, particles remain undistorted. This suggests that the stresses generated by the surrounding nanotube distort the catalyst particle during growth.

1. Introduction

Precise structural control of carbon nanotubes (CNTs) remains one of the key challenges to realizing their technological potential. Plasma-enhanced chemical vapor deposition (PECVD) using catalytic metal nanoparticles enables large-scale growth of CNT films, however, much is still unknown about what happens to the catalyst particle during growth [1–3]. Numerous studies with electron microscopy have captured the dynamics of in situ CNT growth from crystalline catalyst particles [4–9]. In these studies, and in others, conducted ex situ, close inspection of bright-field (BF) transmission electron microscope (TEM) images reveals significant contrast variations along the length of the catalyst particles [10,11]. Sources of contrast variation in BF–TEM images include changes in crystal orientation relative to incident electron beam, strain, or thickness, and can indicate a distorted crystalline structure [12]. We examined, in detail, the crystalline structure of iron carbide catalyst particles found inside the base of multiwall carbon nanotubes using a nano-scale electron probe in the TEM.

2. Experimental

Multiwall carbon nanotubes (MWCNTs) with diameters ranging from 20 to 70 nm were grown using an inductively-coupled plasma and iron catalyst through catalytic PECVD. The iron catalyst was deposited on a native-oxide coated silicon substrate as a 10 nm-thick film using electron-beam evaporation. Before nanotube growth, the iron catalyst film was exposed to a plasma maintained in a mixture of H_2 and Ar (50 sccm H_2 and 5 sccm Ar) at 200 W and 700 °C for 15 min. This hydrogen plasma pretreatment breaks apart the iron film to form nanometer-sized metal islands, and reduces iron oxides present in the catalyst film. Nanotubes were grown at 800 °C and 10 Torr using a 13.56 MHz radio-frequency plasma maintained with 200 W power in a CH_4 (5 sccm), H_2 (5 sccm), and Ar (68 sccm) gas mixture. A dense film of multiwall carbon nanotubes grew to an average length of four microns after 30 min of plasma deposition. Nanotubes were removed from the Si/SiO_2 substrate by sonication in ethanol for 30 s, and then transferred to a copper TEM grid coated with a lacey carbon support film. In some experiments the metal catalyst was deposited directly on SiO_2 TEM grids and carbon nano-

* *Corresponding author:* Fax: +1 612 626 7246.
E-mail address: aydil@umn.edu (E.S. Aydil).
0008-6223/$ - see front matter
doi:10.1016/j.carbon.2010.06.049

tubes were grown and examined on these grids without removing them by sonication. TEM analysis was conducted using an FEI Tecnai F-30 microscope with a Schottky field-emission electron gun operated at 300 keV. Nanoprobe electron diffraction techniques were used to collect convergent-beam electron diffraction (CBED) patterns from nanometer-size regions along the length of individual catalyst particles located inside the base of MWCNTs. Diffraction patterns were recorded using a Gatan charge-coupled device (CCD). This method was instrumental in identification of small-angle rotations between various sections in 5–10 nm thick CdSe quantum rods reported by Yu et al. [13].

3. Results and discussion

Carbon nanotubes grow up with respect to the substrate from catalyst particles, which remain attached to the substrate. Fig. 1 shows an SEM of a bundle of nanotubes, which has partially peeled off from the substrate. Elongated catalyst particles are clearly visible (brighter regions) at the bases of nanotubes where catalysts and nanotubes were attached to the substrate. The thick part of each catalyst is at the bottom of the nanotube, while the crystal becomes thinner as one moves up from the nanotube base. This type of catalyst particle shape change is not common in thermal CVD and mostly seen only with PECVD. The majority of nanotubes have outer diameters between 20 and 40 nm, and appear well graphitized. Only occasional cupping is observed along the nanotube. The majority of the length consists of parallel walls. The crystalline catalyst particle located inside the base of each nanotube exhibits a elongated tear-drop morphology, as is shown in the BF–TEM images in Figs. 2–5. Symmetries and planar spacings in electron diffraction patterns obtained from these catalyst crystals are consistent with the cementite (Fe_3C) phase (orthorhombic space group Pnma No. 62, $a = 0.5008$ nm, $b = 0.4465$ nm, $c = 0.6725$ nm).

All catalyst crystals examined exhibit significant contrast variation along their lengths when imaged under bright- and dark-field conditions. For example, Fig. 2 shows representative BF and dark-field (DF) TEM images of a cementite catalyst single crystal inside the base of a MWCNT oriented with its [1 0 0] zone axis aligned along the electron beam direction. Evident in both images, but more pronounced in the DF image, is the change in contrast along the length of the catalyst crystal even though the particle is a single crystal. Significant contrast variation present along the length of the crystal indicates possible changes in thickness, strain, or orientation of the crystal.

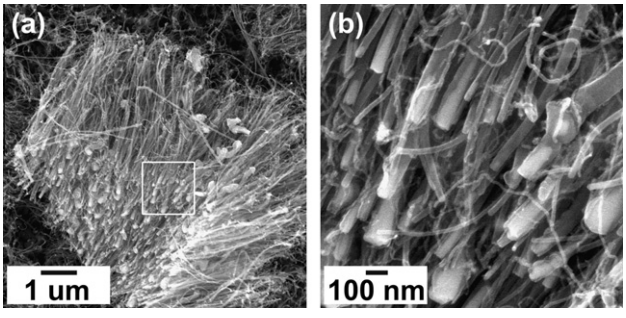

Fig. 1 – (a) SEM image of the base region of the carbon nanotube bundles that have peeled off from the substrate. (b) Same bundle in higher magnification showing elongated catalyst nanocrystals.

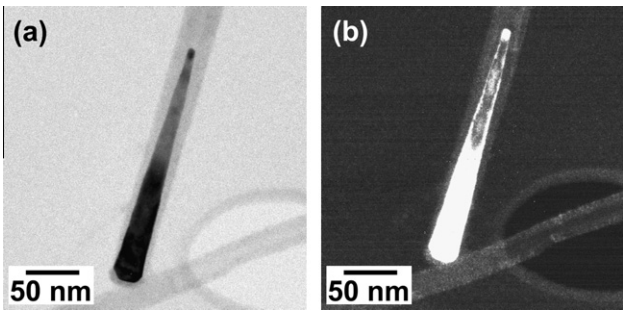

Fig. 2 – (a) BF and (b) DF–TEM images of an oriented cementite catalyst crystal inside the base of a multiwall carbon nanotube. The crystal [1 0 0] zone axis is parallel to the electron beam. The DF image was formed from the 020 spot.

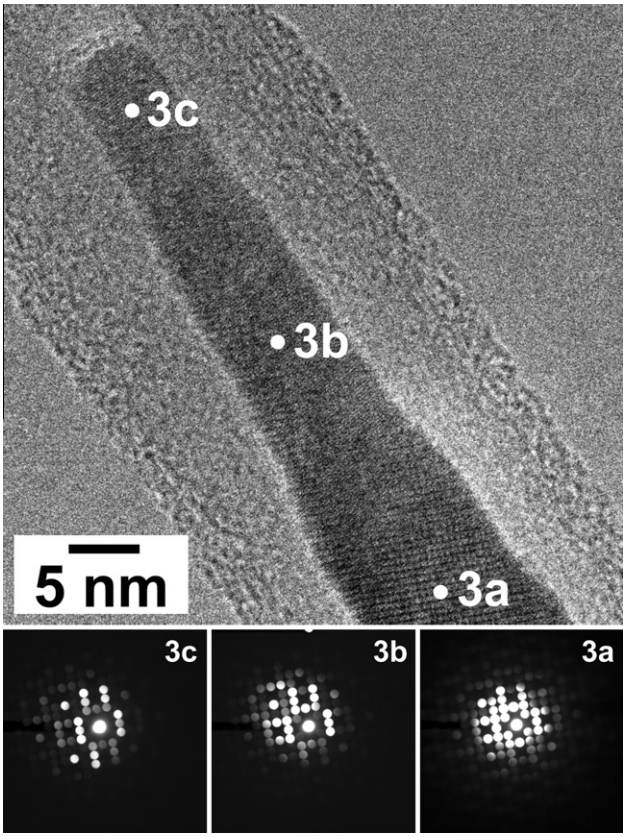

Fig. 3 – BF–TEM image (top) of a cementite crystal approximately 60 nm in length oriented along the [0 0 1] zone axis at position 3a and the CBED patterns (bottom) obtained from positions 3a–c. The CBED intensity distribution changes as the probe is moved from position 3a to positions 3b and 3c, which indicates that the crystal orientation changes along its length.

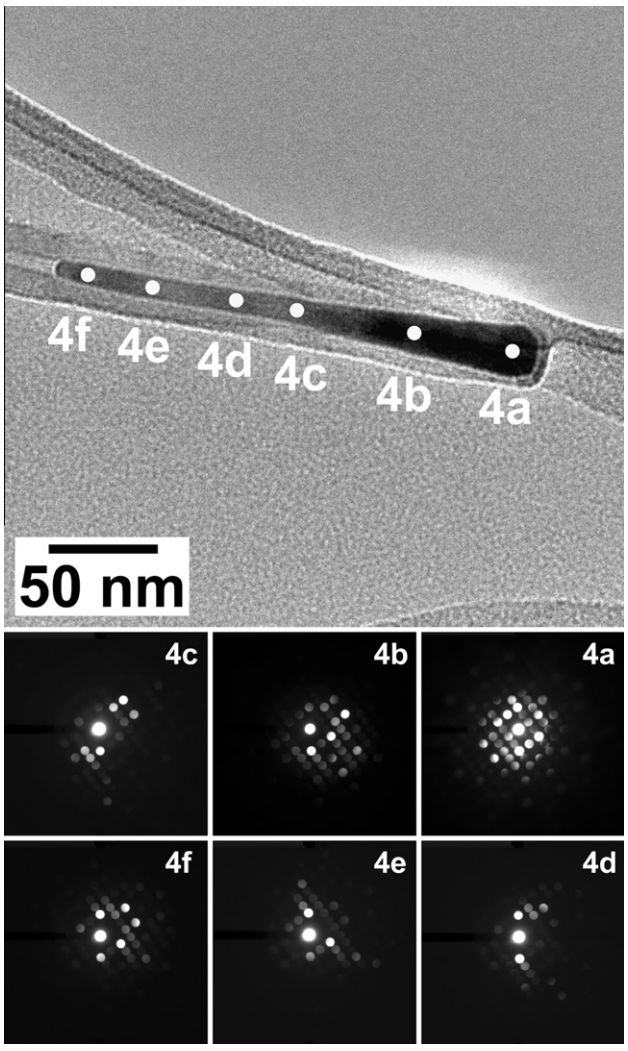

Fig. 4 – BF–TEM image (top) of a 225 nm long cementite crystal oriented along the [1 0 1] zone axis at position 4a and the CBED patterns (bottom) obtained from positions 4a–f. The CBED intensity distribution changes significantly as the probe is moved along the crystal, which indicates a severe change in crystal orientation along its length.

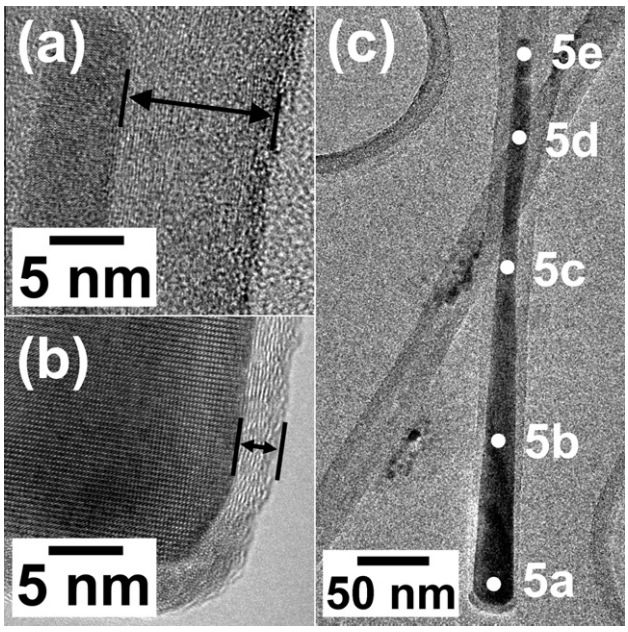

Fig. 5 – HRTEM images comparing the number of graphene walls at the (a) top and (b) bottom region of a catalyst crystal inside the base of a carbon nanotube. Arrows indicate that the number of walls decreases significantly as one moves downwards towards the base of the catalyst crystal. (c) BF–TEM image of a 400 nm long cementite crystal. Initially, the crystal was aligned along the [1 1 1] zone axis at position 5a. Tilt angles (α and β) required to return the crystal back to the same zone axis were recorded at each position 5a–e (see Table 1).

To determine the cause of this variation, a series of CBED patterns were recorded using an electron nanoprobe positioned at different points along the catalyst. Fig. 3 shows CBED patterns obtained from three different positions along a cementite catalyst crystal that was approximately 60 nm in length. An electron probe was initially placed at position 3a, and the crystal was tilted such that the electron beam was aligned with the [0 0 1] zone axis. The probe was then moved along the length of the catalyst and CBED patterns recorded at positions 3b-3c.

Diffraction from position 3a, at the very base of the nanotube, shows full symmetry of the cementite [0 0 1] zone axis, as expected. However, at positions 3b and 3c, the intensity distribution in the diffraction disks changes, which indicates that the orientation of the cementite crystal relative to the incident electron beam has changed. This change in orientation is also evident in the TEM image; the well-resolved lattice image at point 3a changes into less well-resolved lattice fringes at points 3b and 3c as the crystal orientation changes and the zone axis and the electron beam become slightly misaligned.

More severe variations in orientation are observed in longer single crystalline cementite catalyst particles. For example, Fig. 4 shows a series of CBED patterns obtained from six different positions along a crystal that was approximately 225 nm in length. The base (position 4a) of this crystal is oriented along its [1 0 1] zone axis, but as the probe was moved to positions 4b–4f, the intensity distribution in the diffraction disks changed significantly, again indicating changes in crystal orientation. Careful examination of the intensity distributions in the CBED patterns in Figs. 3 and 4 indicates that these changes in orientation are not continuous in the same direction, but are random misorientations as one moves from the base to the tip of the catalyst particle. No visible grain boundaries were observed between sections of different orientation. Each catalyst crystal, therefore, is an imperfect single crystal and exhibits a combination of random rotation, twist, and bend components along its length.

We used nanoprobe diffraction in combination with crystal tilting in the electron microscope to quantify the magnitude of the observed misorientations between different sections of each catalyst crystal. One such measurement is shown in Fig. 5(c) and the results are summarized in Table 1. First, the electron nanoprobe was positioned at the base

Table 1 – α and β tilt angles and the calculated angular differences in crystal misorientation at each position shown in Fig. 5c relative to position 5a.

Position	Alpha (±0.1°)	Beta (±0.1°)	Angular difference (°)
5a	−3.8	−5.1	reference
5b	−4.1	−5.3	0.3
5c	−4.5	−4	1.3
5d	−7.6	−6.2	4
5e	−8.4	−8.3	5.6

(position 5a) of a catalyst crystal that had been tilted using a double-tilt holder to a specific low-index zone axis, [1 1 1] in the case shown in Fig. 5. Second, the nanoprobe was moved along the catalyst to position 5b, where the crystal was now misoriented with respect to this zone axis. Third, the crystal was again tilted to bring the zone axis at position 5b parallel to the electron beam and the angular tilts required to accomplish this realignment were recorded. This process was continued at the remaining positions along the catalyst, and effective angular differences were calculated. Table 1 lists the two angle values of the double-tilt holder (α and β) for each of the five positions along the catalyst particle shown in the BF image of Fig. 5, as well as the calculated angular difference in orientation of the crystal at each spot relative to position 5a. Orientation differences between adjacent sections of catalyst crystals range from 1 to 3°. The unsystematic changes in α and β values are typical and indicative of the random nature of the crystalline misorientations and show that the catalyst particle, although single crystalline, is significantly deformed. However, misorientations at different sections of the crystal are uncorrelated.

We have considered that the deformation of a catalyst crystal might be induced by the electron beam irradiation; however, control experiments eliminated the possibility that nanocrytsals are deforming while in the microscope. For example, diffraction patterns did not change with time over the time scales that crystals were examined. Moreover, diffraction spots in SAED patterns of entire crystals with the electron beam spread substantially showed either small arc segments, or multiple spots instead of single sharp diffraction spots, indicating that the crystal orientation was slightly different over the entire crystal. We estimated the temperature rise of a crystal due to electron irradiation from a converged electron beam using the Bethe expression for mean energy loss of an incident electron [14,15]. Using the maximum current density of $\sim 2\times10^6$ A/cm^2, which represents the highest current density used during all TEM techniques described herein, we find that this temperature rise is less than 1 °C, and is insufficient to change or deform the catalyst particle. These experiments show that the deformation exists in the catalyst crystals before they were put in the microscope and that the electron beam did not alter the sample.

Careful examination of the misorientations along a single catalyst suggests that the surrounding graphene walls exert forces on the catalyst particle to deform it during growth. Catalyst particles exhibit a relatively large region near their attachment point to the substrate, which appears undistorted and does not change in orientation. This is evident from the large constant (dark) contrast region at the base of each catalyst particle in the BF–TEM images of Figs. 2–5, and by the large bright region in the associated DF–TEM image in Fig. 2. Farther away from the base, where the crystal orientation has changed, the catalyst crystal appears lighter in the BF image and darker in the DF image. Examination of the carbon nanotube structure that encapsulates the crystal reveals that the number of graphene walls near the base region decreases dramatically, as is evident in the HRTEM images of Fig. 5(a) and (b). In many cases, the graphene walls do not extend completely to the end (base) of the catalyst crystal. Crystal faceting is observed where the tube walls terminate. In contrast, away from the base and farther up into the tube, the number of walls increases. Sun et al. estimated pressures exerted by multiwall carbon onions and nanotubes on encapsulated metal particles in heating and electron irradiation experiments to be 10–30 GPa [16]. In separate early-growth experiments, we found that catalyst crystals lose their pronounced faceting and exhibit strain contrast once they became encapsulated in graphene layers. Fig. 6 shows such an example that has been observed during initial stages of carbon nanotube growth on SiO_2 TEM grids. Such an experiment simulates carbon nanotube growth on native oxide covered silicon but the catalyst can be observed in cross section without disturbing it by sonication. Fig. 6(a) shows that before graphene layers form on the catalyst, the nanocrystals are faceted. Once graphene layers form, the portion of the catalyst that is encapsulated by graphene loses its faceted shape and become rounded. Moreover, the region adjacent to the

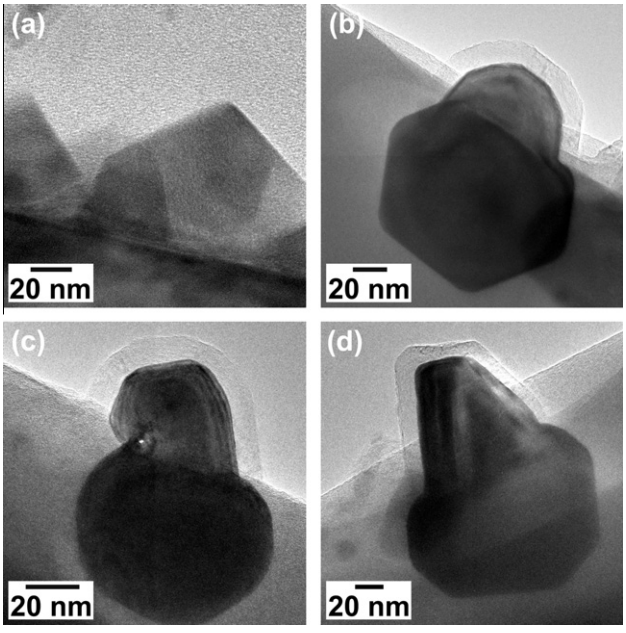

Fig. 6 – TEM images of (a) a catalyst nanoparticle before growth and (b–d) after nucleation of graphene layers. Before growth the catalyst nanoparticle is faceted. After growth of graphene layers the catalyst faces encapsulated by graphene layers lose their faceted shape and catalyst exhibits strain contrast in the TEM. The regions not covered by graphene walls retain their facets.

graphene walls exhibits strain contrast in the TEM. In contrast, the regions not covered by graphene walls remain faceted. This shows that indeed it is the surrounding walls that deform the catalyst. Such deformations have also been seen in carbon-onion encapsulated metal crystals [17]. The lowest melting point in the Fe–C phase diagram in the composition region of interest is 1147 °C, the eutectic temperature. While this temperature is well above the growth temperature and we do not expect the catalyst crystal to melt based on the phase diagram, we cannot discount surface melting, particularly in presence of stress. We confirmed that the faceted morphology in and the rounded morphology in Fig. 6(b) belong to the same crystal: the convergent-beam electron diffraction from the region with the facets and the region with the carbon sheath are the same indicating that either they are two crystals oriented the same way sitting on top of each other or they are the same crystal. The former is very low probability and we have found other crystals that exhibit similar morphology [Fig. 6c and d]. Careful examination of TEM in Fig. 6(b) also shows a stress contour (contrast) that is continuous between the faceted and rounded regions of the crystal. This could only happen if the two regions belonged to the same crystal.

These observations suggest that the catalyst particles are subjected to significant stresses by graphene layers that surround them. It seems reasonable to conclude that the observed shape and misorientation of the cementite catalyst crystals along their length is due to the compressive stresses generated by the surrounding graphene layers. The catalyst particles are either still under stress exerted by the graphene layers or have been subjected to significant stresses sometime during growth. In the former case, and if the deformation is in the elastic regime, etching the graphene layers may help the crystal recover from the deformation. In the latter case, the crystal deformation is irreversible and will remain even after removing the carbon sheath."

Observations of random small-angle rotations, twists, and bends of the catalyst crystal may have significant implications on the structure of the nanotube that it produces. Recent in situ TEM studies have captured carbon nanotube walls growing from individual metal crystalline catalyst particles [4–9]. Close inspection of these catalyst crystals from BF images reveals non-uniform changes in diffraction contrast across the crystals, as well as the appearance and disappearance of lattice fringes covering partial sections of the crystals. These observations indicate that small sections of the catalyst are being rotated, twisted, or bent by the growing carbon nanotube. If the catalyst crystal acts as a template for carbon atoms to form graphene walls of the nanotube, then a significant number of defects and strain may be introduced whenever a portion of the catalyst is deformed and changes orientation. This may also cause tube growth to change direction, as observed here and by others [18]. It is also interesting to note that, recently, Ding et al. presented a screw dislocation mechanism for nanotube growth where the nanotube was observed to rotate as it grew [19]. While the relation between Ding's observation and the catalyst rotation, twisting and bending reported herein is unclear, it is not difficult to imagine that such a mechanism may rotate and twist the catalyst.

4. Conclusions

In conclusion, a nanoprobe electron beam in the TEM was used to obtain CBED patterns from nanometer-size regions along the lengths of individual cementite catalyst crystals located inside the base of multiwall carbon nanotubes. Random small-angle (1°–3°) misorientations between adjacent sections along catalyst crystals indicate that the carbon nanotubes exert stresses that rotate, twist, and bend small sections of the catalyst during growth. These findings may have significant implications on the ability to control carbon nanotube structure using catalytic PECVD.

Acknowledgements

The authors thank Dr. O. Ugurlu for technical support. This material is based primarily upon work supported by the National Science Foundation (NSF) grant CBET-0613629. Part of this work was carried out in the College of Science and Engineering Characterization Facility, at the University of Minnesota, which receives partial support from the NSF-NNIN program and capital equipment funding from the National Science Foundation through the MRSEC, ERC and MRI programs.

REFERENCES

[1] Ren ZF, Huang ZP, Xu JW, Wang JH, Bush P, Siegal MP, et al. Synthesis of large arrays of well-alligned carbon nanotubes on glass. Science 1998;282(5391):1105–7.
[2] Meyyappan M, Delzeit L, Cassell A, Hash D. Carbon nanotube growth by PECVD: a review. Plasma Sources Sci T 2003;12(1–2):205–16.
[3] Melechko AV, Merkulov VI, McKnight TE, Guillorn MA, Klein KL, Lowndes DH, et al. Vertically aligned carbon nanofibres and related structures: controlled synthesis and directed assembly. J. Appl. Phys. 2005;97(4):041301.
[4] Helveg S, Lopez-Cartes C, Sehested J, Hansen PL, Clausen BS, Rostrup-Nielsen JR, et al. Atomic-scale imaging of carbon nanofibre growth. Nature 2004;427(6973):426–9.
[5] Rodriguez-Manzo JA, Terrones M, Terrones H, Kroto HW, Sun LT, Banhart F. Nat. Nanotechnol. 2007;2(5):307–11.
[6] Schaper AK, Hou HQ, Greiner A, Phillipp F. The role of iron carbide in multiwalled carbon nanotube growth. J. Catal. 2004;222(1):250–4.
[7] Yoshida H, Takeda S, Uchiyama T, Kohno H, Homma Y. Atomic-scale in-situ observation of carbon nanotube growth from solid state iron carbide nanoparticles. Nano Lett. 2008;8(7):2082–6.
[8] Hofmann S, Sharma R, Ducati C, Du G, Mattevi C, Cepek C, et al. In situ observations of catalyst dynamics during surface-bound carbon nanotube nucleation. Nano Lett. 2007;7(3):602–8.
[9] Begtrup GE, Gannett W, Meyer JC, Yuzvinsky TD, Ertekin E, Grossman JC, et al. Facets of nanotube synthesis: High-resolution transmission electron microscopy study and density functional theory calculations. Phys. Rev. B 2009;79(20):205409.
[10] Yao Y, Falk LKL, Morjan RE, Nerushev OA, Campbell EEB. Synthesis of carbon nanotube films by thermal CVD in the presence of supported catalyst particles Part I: The silicon

substrate/nanotube film interface. J. Mater. Sci: Mater. Electron. 2004;15(8):533–43.
[11] Kim H, Sigmund W. Iron particles in carbon nanotubes. Carbon 2005;43(8):1743–8.
[12] Williams DB, Carter CB. Transmission Electron Microscopy: A Textbook For Materials Science. New York: Plenum Press; 1996.
[13] Yu ZH, Hahn MA, Maccagnano-Zacher SE, Calcines J, Krauss TD, Alldredge ES, et al. Small-angle rotation in individual colloidal CdSe quantum rods. ACS Nano 2008;2(6): 1179–88.
[14] Mkhoyan KA, Silcox J, McGuire MA, Disalvo FJ. Radiolytic purification of CaO by electron beams. Phil. Mag. 2006;86(19):2907–17.
[15] Kohl H, Reimer L. Transmission Electron Microscopy Physics of Image Formation. New York, NY: Springer-Verlag; 2008.
[16] Sun L, Rodriguez-Manzo JA, Banhart F. Elastic deformation of nanometer-sized metal crystals in graphitic shells. Appl. Phys. Lett. 2006;89(26):263104.
[17] Sun LT, Krasheninnikov AV, Ahlgren T, Nordlund K, Banhart F. Phys. Rev. Lett. 2008;101(15):156101.
[18] Yoshida H, Uchiyamai T, Takeda S. Environmental transmission electron microscopy observations of swinging and rotational growth of carbon nanotubes. Jpn. J. Appl. Phys. 2 2007;46(36–40):L917–9.
[19] Ding F, Harutyunyan AR, Yakobson BI. Dislocation theory of chirality-controlled nanotube growth. Proc. Natl. Acad. Sci. USA 2009;106(8):2506–9.